Near-infrared Characterization of Four Massive Stars in Transition Phases*

Yanina R. Cochetti[1,2] , Michaela Kraus[3] , María L. Arias[1,2], Lydia S. Cidale[1,2], Tõnis Eenmäe[4], Tiina Liimets[3,4] ,
Andrea F. Torres[1,2], and Anlaug A. Djupvik[5]

[1] Departamento de Espectroscopía, Facultad de Ciencias Astronómicas y Geofísicas, Universidad Nacional de La Plata, Paseo del Bosque S/N, La Plata, B1900FWA,
Buenos Aires, Argentina; cochetti@fcaglp.unlp.edu.ar
[2] Instituto de Astrofísica de La Plata (CCT La Plata - CONICET, UNLP), Paseo del Bosque S/N, La Plata, B1900FWA, Buenos Aires, Argentina
[3] Astronomical Institute, Czech Academy of Sciences, Fričova 298, 25165 Ondřejov, Czech Republic
[4] Tartu Observatory, University of Tartu, 61602 Tõravere, Tartumaa, Estonia
[5] Nordic Optical Telescope, Rambla José Ana Fernández Pérez 7, E-38711 Breña Baja, Spain

Abstract

Massive stars typically undergo short-lived post-main-sequence evolutionary phases with strong mass loss and occasional mass eruptions. Many of such massive stars in transition phases have been identified based on their dusty envelopes. The ejected material often veils the stellar photospheres so that the central stars cannot be assigned proper spectral types and evolutionary stages. The infrared spectral range has proved to be ideal for the classification of evolved massive stars and for the characterization of their environments. To improve our knowledge on the central stars of four such dust-enshrouded objects, [GKF 2010] MN 83, [GKF 2010] MN 108, [GKF 2010] MN 109, and [GKF 2010] MN 112, we collect and present their first medium-resolution K-band spectra in the 2.3–2.47 μm region and discuss the location of the stars in the JHK color–color diagram. We find that the emission-line spectra of both MN 83 and MN 112 show characteristics typically seen in luminous blue variable (LBV) stars. In addition, we propose that the presence and strength of the newly reported Mg II lines might be used as a new complementary criterion to identify LBV candidates. The spectra of the other two objects imply that MN 108 is an O-type supergiant, whereas MN 109 could be an LBV candidate in its active phase. We derive lower limits for the reddening toward the stars and find that three of all dereddened fall into the region of confirmed LBVs.

Unified Astronomy Thesaurus concepts: Early-type emission stars (428); Circumstellar matter (241)

1. Introduction

For most of their life massive stars interact with their environments through high-density stellar winds. They add chemically processed material into the interstellar medium (ISM) and modify the dynamics of their neighborhood, depositing momentum and energy. After massive stars leave the main sequence, they can evolve through individual short-lived transition phases of intense mass loss or eruption events before ending their lives as supernovae. Moreover, as the stellar evolution is sensitive to the mass loss (Smith 2014), the amount of mass lost in each stage affects the subsequent evolution of the star (Maeder et al. 1980; Meynet & Maeder 2005; Georgy 2012). Despite their importance on the fate of massive stars, some short transition phases are not reproducible with the currently available evolution models. In this context, to improve our comprehension of stellar and galactic evolution, a better understanding of massive stars in transition phases is vital (Langer et al. 1994; Puls et al. 2008; Langer 2012).

As a result of the high mass loss or mass eruptions, massive stars in transition phases usually present large amounts of circumstellar material in the form of disks, shells, or rings, with physical conditions that allow for the formation of dust and molecules. This circumstellar material often hides the stellar photosphere, so that it can be difficult to assign proper spectral types and to determine the evolutionary stage of the central star. Nevertheless, the material around the star provides information about the kinematics and the history of the mass loss through specific atomic and molecular emission features.

One class of transition objects is composed of the luminous blue variables (LBVs; see Conti 1997, for a definition of the phenomena). Their progenitors are very massive and luminous stars. However, the physical state of these stars prior to or after the LBV phase is not well constrained, but seems to depend on the initial mass of the star. While the most massive stars ($M > 40\,M_\odot$) seem to develop into LBVs shortly after they left the main sequence, their lower-mass counterparts ($M < 40\,M_\odot$) seem to turn into LBVs only after they have passed through the red supergiant phase (Meynet et al. 2011).

LBVs possess relatively slow dense winds, with high mass-loss rates. Moreover, most LBVs are surrounded by a nebula, presenting a wide range of morphologies, from ring-like shells to bipolar lobes and triple-ring systems (Nota et al. 1995; Weis 2001; Smith 2007). These nebulae are most likely formed from material ejected either during a giant eruption or from phases of enhanced mass loss during the so-called S Dor cycles. Starting from a regular blue supergiant (BSG) stage (quiescent state), the star apparently develops into a cool A- or F-type supergiant (outburst). During such an S Dor outburst, which can last from years to decades (van Genderen et al. 1997), the

---

mass-loss rate can be increased by up to a factor of five (Stahl et al. 2001; Groh et al. 2008) before the star finally returns into its quiescence state as a regular BSG. Only if a star has experienced a giant eruption or a full S Dor cycle is it classified as LBV; otherwise, it is classified only as a candidate LBV (cLBV).

Another group in transition comprises the B[e] supergiants (B[e]SGs). These luminous ($4 < \log L/L_\odot < 6$) emission-line stars form a subset of the early-type supergiants. Stars within this group are known for their peculiar spectral character, suggesting a complex circumstellar environment. Their optical spectra display intense and broad emission lines of the Balmer series along with narrow emission lines of neutral and singly ionized metals in both permitted and forbidden transitions (Cannon 1924; Henize 1956; Smith 1957; Feast et al. 1960). Moreover, these objects possess an intense near-infrared excess owing to hot circumstellar dust (Allen & Glass 1976; Glass 1977; Stahl et al. 1983, 1984). The observed peculiarities can be understood in terms of a coexistence of high-ionized polar winds, also traced by the broad blueshifted UV resonance lines of highly ionized elements, and equatorial rings or disks (Zickgraf et al. 1985). The circumstellar rings/disks consist of low-ionized or neutral atomic material (Kraus et al. 2007, 2010; Aret et al. 2012), hot molecular gas, and warm dust (McGregor et al. 1988; Morris et al. 1996; Kastner et al. 2006, 2010; Meilland et al. 2010; Wheelwright et al. 2012; Kraus et al. 2013). This disk material is in quasi-Keplerian rotation and clearly detached from the central star (Aret et al. 2012, 2016; Cidale et al. 2012; de Wit et al. 2014; Kraus 2017; Kraus et al. 2017; Maravelias et al. 2018).

In contrast to the LBVs, most B[e]SGs are not reported to possess large-scale ejecta. The only exceptions so far are the three Galactic objects MWC 137 (Marston & McCollum 2008; Kraus et al. 2017), MWC 314 (Marston & McCollum 2008), and MWC 349A (Gvaramadze & Menten 2012; Kraus et al. 2020).

These two different groups of stars (LBVs and B[e]SGs) occupy similar regions in the H-R diagram (Aret et al. 2012), and to assign a star a classification as either LBV or B[e]SG is not trivial. Candidates for these two groups are identified through spectroscopic features or circumstellar structures similar to the ones associated with these types of evolved massive stars (e.g., Clark et al. 2003, 2012). However, optical and IR features observed in the spectra of B[e]SGs and LBVs in quiescence are practically indistinguishable (Oksala et al. 2013), and only subtle details could be used for a proper classification. For instance, emission from [O I] and [Ca II] lines, or CO bands, is characteristic for B[e]SGs (Kraus 2019; see also Section 5). In addition, these two classes of stars can be separated based on their distinct locations in infrared color–color diagrams (Oksala et al. 2013; Kraus 2019). However, the lack of photometric measurements, along with full spectral coverage, often hampers a proper stellar classification. This is especially true for the large number of recently identified evolved massive stars embedded within dense infrared shells (Gvaramadze et al. 2010a, 2010b, 2012; Wachter et al. 2010).

In this work we study four objects with infrared shells, listed in Gvaramadze et al. (2010a) and proposed to host either a BSG or a cLBV as the central source. To reinvestigate and to improve their classification, we present and analyze the medium-resolution K-band spectra of these objects. As has been shown by many authors (see, e.g., Kraus et al. 2014; Liermann et al. 2014; Arias et al. 2018; Kourniotis et al. 2018),

spectral features in the near-infrared provide valuable complementary information for the classification of massive stars in transition phases. In addition, we present optical spectra and photometric measurements for two of them. Optical narrow-band images are obtained for all four, and near-infrared images for two targets. Our goal is to obtain supplementary information about the circumstellar material that can help to define the possible evolutionary states of the central objects.

2. The Selected Sample

From the catalog of Gvaramadze et al. (2010a) of evolved massive stars with infrared nebulae, we selected the four northern objects that have been proposed to host either a BSG or a cLBV as the central source. In this section, we briefly describe these objects based on the literature status.

[GKF 2010] MN 83: Using images from Spitzer Infrared Array Camera (IRAC) and Very Large Array, Davies et al. (2007) found a bright ring nebula in 8 μm and 20 cm, respectively, with a highly reddened star at its center (see their Figure 21). These authors associated the nebula with the source IRAS 18367−0556 (Becker et al. 1994) and remarked that this object is very similar to the cLBV HD 168625 (Robberto & Herbst 1998). The bulk of the radio emission at 1.4 GHz reported by Condon et al. (1998) is in the southwestern part of the dust ring, rather than aligned with the central star. Then, it is improbable that the radio emission comes from the ionized stellar wind. Instead, the radio emission might originate from the ionization of the surrounding ejecta because of the presence of a hot central star, or from a fast wind pushing a slower, dusty wind ejected in a cooler phase of the star.

Gvaramadze et al. (2010a) reported an ellipsoidal nebula with a size of $30'' \times 45''$ in the Multiband Imaging Photometer for Spitzer (MIPS) 24 μm images, with a radio counterpart at 20 cm. These authors included this source in their catalog as MN 83 and classified it as a cLBV, based on the work of Davies et al. (2007).

Using Chandra observations, Nazé et al. (2012) confirmed the nondetection of X-ray emission from MN 83. The closest X-ray source is the BSG GAL 026.47+00.02 situated at a distance of ∼30″.

[GKF 2010] MN 108: Gvaramadze et al. (2010a) discovered a bipolar nebula on Spitzer MIPS images with a size of $50'' \times 50''$. These authors also reported strong optical absorption lines of H I and He I and numerous absorption lines of He II, with the strongest being He II $\lambda4686$ and He II $\lambda5412$. They classified this object as a BSG star.

[GKF 2010] MN 109: Phillips & Ramos-Larios (2008) identified a ring-like structure around the star (which they named G052.4-00.0 in their paper) based on images from the Spitzer GLIMPSE mid-IR survey of the galactic plane and the MIPS 24 μm images. This ring-like structure has not been detected either in the IRAS survey or in DSS images. Neither have radio measurements been performed so far. The central star is seen, however, in the near-IR Two-Micron All-Sky Survey (2MASS), based on which Phillips & Ramos-Larios (2008) concluded that the central star is an early-type supergiant at a distance of ∼8 kpc from the Sun. It is associated with nearby regions of star formation. The radius of the infrared ring is of the order of ≈0.3 pc, and the extinction A_V toward the central star is of the order of 21 mag. Gvaramadze et al. (2010a) included MN 109 in their catalog as a BSG candidate with an ellipsoidal nebula having a size of $15'' \times 20''$.

Table 1
Observed Stellar Sample: Identification Number, Equatorial Coordinates (R.A. α and Decl. δ), and Observing Log

ID [GKF 2010]	α [J2000]	δ [J2000]	IR Spectra			Optical Spectra		
			Obs. Date	Exp. Time (s)	S/N	Obs. Date	Exp. Time (s)	S/N
MN 83	18:39:23.01	−05:53:19.9	2014 May 9	8	200	190	⋯	⋯	⋯
MN 108	19:26:58.96	+18:46:44.0	2014 Jul 5	20	280	120	2019 Aug 13	1800	40
MN 109	19:28:14.58	+17:16:23.1	2014 Mar 20	8	630	220	⋯	⋯	⋯
MN 112	19:44:37.60	+24:19:05.9	2013 Jul 7	8	192	270	2019 Aug 13	3600	100

[GKF 2010] MN 112: This object is listed in the catalog of Hα emission stars in the northern Milky Way (Kohoutek & Wehmeyer 1999). Associated with this object, Gvaramadze et al. (2010a) identified a round nebula with a diameter of 100″, which is also visible at 24 μm (Wachter et al. 2010). Its morphology resembles that of the circumstellar nebula of the Galactic cLBV GAL 079.29+11.46. The optical spectrum of MN 112 is dominated by strong emission lines of H I and He I and numerous lines of N II, Fe III, and Si II. Based on the observed H I and He I emission lines, Wachter et al. (2010) classified it as a B-type star (∼B0–B5). Due to the resemblance of its optical spectrum to the one of the LBV star P Cygni (Gvaramadze et al. 2010b), Stringfellow et al. (2012) and Gvaramadze et al. (2012) assign this object a cLBV status.

3. Observations

3.1. Spectroscopy

Infrared spectra in the K-band were obtained with the Gemini Near Infrared Spectrograph in long-slit mode. The selected instrumental configuration was a 111 line mm^{-1} grating, a 0″3 slit, and the short camera (0″15 pixel^{-1}). This configuration provides a spectral resolution of $R \sim 6000$ in the spectral range 2.29–2.48 μm. For each target, several ABBA sequences were taken. A late B-type or early A-type star was observed near in time and sky position to perform the telluric absorption correction. Flats and arcs were taken with every science target. The data reduction steps include the subtraction of the AB pairs, flat-fielding, telluric correction, and wavelength calibration. The reduction process was carried out with the IRAF[6] software package.

Optical spectroscopic observations were done with the 1.5 m telescope AZT-12 at Tartu Observatory of Tartu University, Estonia, using the long-slit spectrograph ASP-32 with a 300 line mm^{-1} grating. This instrumental setting yields a spectral resolution of $R \sim 1000$ in the 4000–7300 Å spectral range.

The spectroscopic observing log is given in Table 1.

3.2. Photometry

Photometric observations were carried out with the 0.31 m Planewave CDK12.5 telescope at Tartu Observatory. The telescope is equipped with an Apogee Alta U42 CCD-camera and Astrodon Photometrics B, V, R_C, and I_C Bessell filters. All observations were calibrated by zero, dark, and flat frames. For measurements and transformations to the Johnson–Cousins standard system, the AVSO's VPHOT service was used.

Comparison stars were selected from the APASS[7] survey data release 10. R_C and I_C magnitudes of the comparison stars were calculated from SLOAN r and i filter measurements of APASS, using relationships described in Jester et al. (2005).

The exposure times for the photometric measurements in the four filters were 180, 120, and 60 s for the stars MN 83, MN 108, and MN 112, respectively. MN 109 was observed purely in the I_C filter with an exposure time of 300 s.

3.3. Imaging

Our objects were additionally observed with the Nordic Optical Telescope (NOT) using the Andalucia Faint Object Spectrograph and Camera (ALFOSC) between 2019 September 5 and 2020 June 20. The observations have been carried out with the narrowband Hα filter with a central wavelength of 6577 Å and an FWHM of 180 Å, covering the emission lines Hα $\lambda6562.82$ and [N II] $\lambda\lambda6548, 6583$. The pixel scale of ALFOSC is 0″21 pixel^{-1}, and the field of view (FOV) is 6′4 × 6′4. The ALFOSC data were processed (biased, flat-fielded, combined) using the standard routines in IRAF. The total exposure time for each target was 30 minutes.

In addition, NOT's near-IR Camera and spectrograph (NOTCam[8]) was used with the Brγ narrowband filter (NOT #209) centered at 2.163 μm to map MN 83 on 2019 September 13 and MN 112 on 2020 June 24. The NOTCam detector is a Hawaii 1k HgCdTe IR array with which the wide-field camera gives a pixel scale of 0″234 pixel^{-1} and an FOV of 4′ × 4′. The observations were obtained in beam-switch mode with an additional small-step dither owing to the search for faint extended emission and the rather dense stellar fields. Every exposure consists of a pixel-by-pixel linear regression of a number of nondestructive reads, sampling the signal up the ramp until the exposure time is reached. For MN 83 we used 50 s exposures, and for MN 112 we used 32 s. Each exposure was flat-fielded, sky subtracted, distortion corrected, and shifted using the NOTCam IRAF package (see footnote 8). The sky was evaluated with the OFF-source frames, and the flat field was obtained from differential twilight flats. The final images were obtained by "median" combining all exposures, leading to total exposure times of 450 s for MN 83 and 576 s for MN 112.

To supplement our images, Spitzer's IRAC (Fazio et al. 2004) images in all four bands (3.6, 4.5, 5.8, and 8.0 μm) and the MIPS (Rieke et al. 2004) in the two bands (24 and 70 μm) were downloaded from the NASA/IPAC Infrared Science Archive. The IRAC images have a pixel scale of 0″6 pixel^{-1}, and MIPS images have 2″45 pixel^{-1}.

---

[6] IRAF is distributed by the National Optical Astronomy Observatory, which is operated by the Association of Universities for Research in Astronomy (AURA) under cooperative agreement with the National Science Foundation.

[7] https://www.aavso.org/apass
[8] See http://www.not.iac.es/instruments/notcam/ for info on NOTCam and for info related to data reduction packages in IRAF.
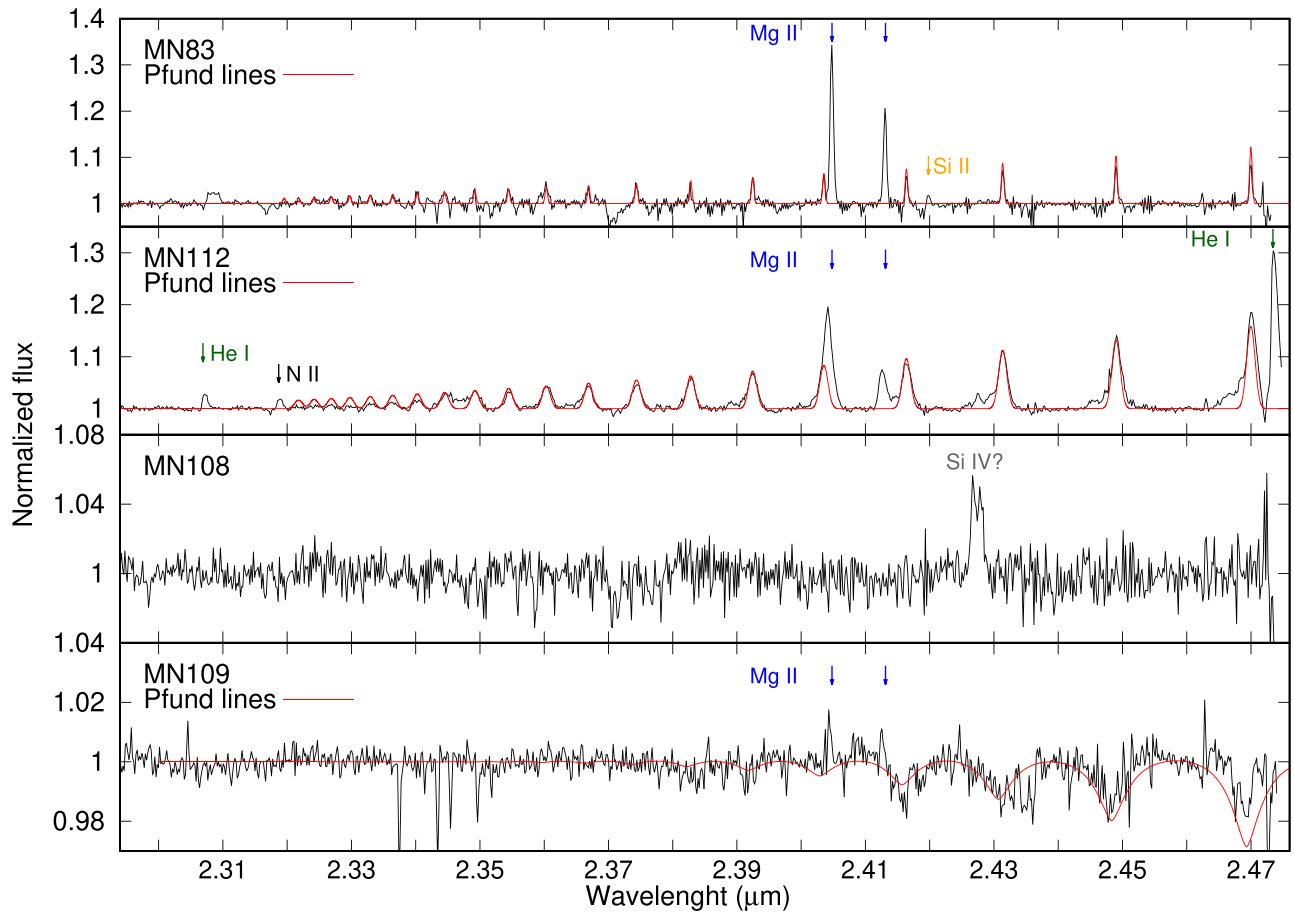
Figure 1. *K*-band spectra from our stellar sample. The hydrogen Pfund series is in emission in MN 83 and MN 112 and in absorption in MN 109. Synthetic spectra (modeled with the code from Kraus et al. 2000 for MN 83 and MN 112, and from a Kurucz 1979 model of a star with $T_{eff} = 10,000$ K and $\log g = 3.0$ for MN 109) are plotted in red. The arrows point out other intense spectral lines observed in this spectral range.
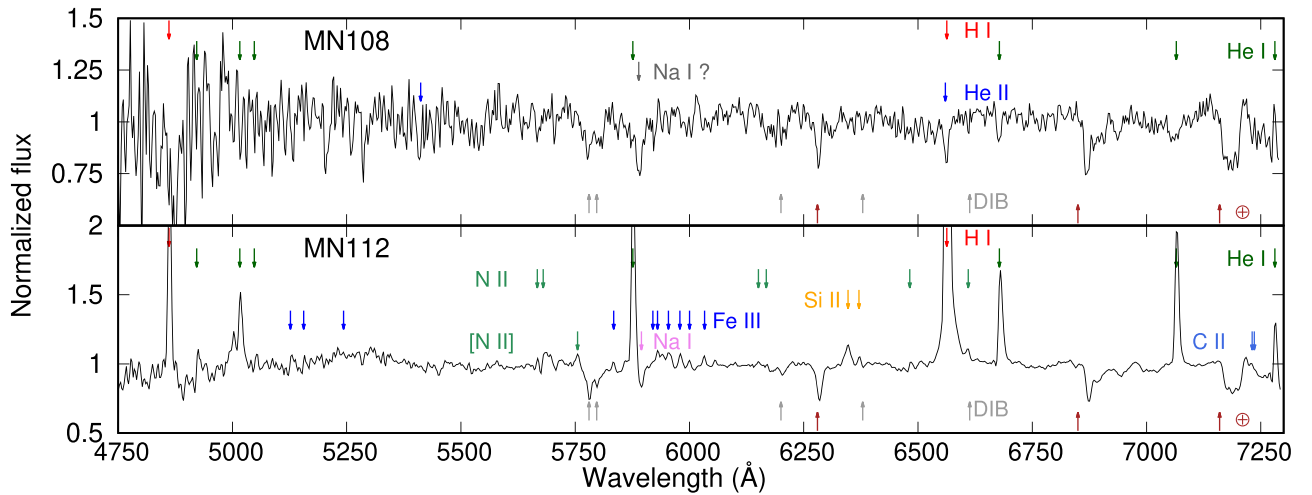

Figure 2. Optical spectra of MN 108 and MN 112. The arrows point out the position of the most intense identified lines, together with the position of the identified diffuse interstellar bands and the telluric bands (pointed out with the symbol ⊕).

4. Results

4.1. Spectroscopy

We present our IR and optical spectra in Figures 1 and 2, respectively, and the photometric measurements in Table 2. For all objects, these are the first medium-resolution *K*-band spectra in the 2.3–2.47 μm region that have been reported.

Inspection of Figure 1 reveals that, obviously, none of the stars display CO bands, neither in emission nor in absorption.

The *K*-band spectra of MN 83 and MN 112 are similar at first glance. Both present emission from the hydrogen Pfund series and from the lines of Mg II 2.4047 and 2.4131 μm. The latter are even more intense than the hydrogen lines. Despite these similarities, there are also differences between these two

Table 2
Johnson–Cousins BVR_CI_C Photometry and IR Colors (Based on Their 2MASS Magnitudes) of Our Stellar Sample

ID	B	V	R_C	I_C	$J - H$	$H - K_s$
MN 83	⋯	⋯	>15.5[a]	⋯	0.545 ± 0.041	0.320 ± 0.040
MN 108[b]	18.430 ± 0.343	16.107 ± 0.343	14.823 ± 0.048	13.521 ± 0.050	2.241 ± 0.062	1.132 ± 0.045
MN 109	⋯	⋯	>18.5[c]	⋯	0.841 ± 0.045	0.598 ± 0.045
MN 112[d]	17.054 ± 0.099	14.538 ± 0.092	12.710 ± 0.029	11.128 ± 0.024	3.096 ± 0.067	1.695 ± 0.057

Notes.
[a] Fainter than $G_{RP} = 15.5$.
[b] $B = 17.69$, $V = 15.52$, $R_C = 15.53$ (Gvaramadze et al. 2010a).
[c] Fainter than $G_{RP} = 18.5$.
[d] $B = 16.42$, $V = 14.64$, $R_C = 13.68$ (Gvaramadze et al. 2010a).

spectra. First, the emission lines in MN 83 are extremely narrow, suggesting that the emission in MN 83 might arise in a nebula. Second, the K-band spectrum of MN 112 also displays the lines of He I 2.3070 μm and He I 2.4734 μm and an emission feature at 2.3187 μm that could be N II. The emission of He I lines suggests that the central star in MN 112 is most likely of spectral type O, whereas MN 83 seems to host a B-type central source. The latter object has only one extra feature, an emission line at 2.42 μm, which might be identified as due to either Si II 2.4199 μm or Ar II 2.4203 μm. All other features are likely artifacts resulting from the extraction process and telluric remnants.

The hydrogen Pfund emission lines are associated with the presence of a hot, dense, and ionized gas, in the form of either a nebula or a wind. To determine some physical parameters of the hydrogen line-forming regions, we used the code developed by Kraus et al. (2000) and modeled the spectra of the Pfund series of MN 83 and MN 112. For the computations we assume that the Pfund lines are optically thin and follow Menzel's case B recombination theory (Menzel et al. 1938). We fix the electron temperature at $T_e = 10{,}000$ K (a typical value for an ionized wind or nebula; see Leitherer & Robert 1991). The shape of the emission lines can be represented with a Gaussian profile. The width of the lines of MN 112 is ~50 km s^{-1} and hence of the order of the spectral resolution, but it is smaller for the case of MN 83. The maximum observed member of the series (n_{max}) is similar in both objects: Pf$_{38}$ for MN 83 and Pf$_{37}$ for MN 112. With those n_{max} values we derived hydrogen densities of $n_H = (6.7 \pm 1.1) \times 10^{13}$ cm^{-3} and $n_H = (7.8 \pm 1.2) \times 10^{13}$ cm^{-3} within the Pfund line-forming regions of MN 83's nebula and MN 112's wind, respectively.

The K-band spectrum of MN 108 displays only a single but evident, apparently double-peaked emission line around 2.427 μm. This line could correspond to a blend of two Si IV 2.4266 and 2.4278 μm lines, reported in emission in late O supergiants by Lenorzer et al. (2002), but because of the absence of other emission lines, we cannot identify it with confidence. Other than that, the IR spectrum of MN 108 appears featureless.

MN 109 presents weak and wide absorption lines in the 2.41–2.47 μm range that correspond to the hydrogen Pfund series. To guide the eye, we overplotted a synthetic spectrum of a star with $T_{eff} = 10{,}000$ K and $\log g = 3.0$, obtained using the *synspec* code (Hubeny & Lanz 2011) with Kurucz (1979) models. The spectrum shows weak and narrow Mg II 2.4047 and 2.4131 μm lines in emission. The little emission features at ~2.31 and ~2.37 μm are residue from the telluric correction.

Only two stars had optical counterparts so that we could obtain a spectrum at optical wavelengths. These are the stars MN 108 and MN 112. In Figure 2 we point out the position of the more intense identified lines, together with the position of the diffuse interstellar bands and telluric bands.

The optical spectrum of MN 108 shows lines of H I, He I, and He II in absorption and resembles the one shown by Gvaramadze et al. (2010a). The presence of He II lines indicates a spectral type O, in line with the results from the K-band spectrum. The absorption feature observed at $\lambda \sim 5889$ Å is most likely a blend of the He I λ5875.62 line with the Na I $\lambda\lambda$5889.95, 5895.92 doublet.

The optical spectrum of MN 112 presents several strong emission lines, dominated by hydrogen and He I. It is practically the same as that obtained by Gvaramadze et al. (2010b, extremely similar to the spectrum of P Cygni), and the equivalent widths of the main emission lines remain the same.

We would like to add that neither of the two stars displays emission of [O I] in their optical spectra, which is one of the defining characteristics of B[e] stars.

4.2. Photometry

Turning now to the photometric measurements, our observations confirm that MN 83 and MN 109 have no optical counterpart. Both stars remained undetected on our $BVR_C I_C$ images owing to the possibly very high extinction toward these sources (see Section 5.3). Through a comparison with the source Gaia DR2 4256466388864127104, which is the faintest source in the same FOV with a Gaia magnitude (G_{RP}) measurement, we conclude that MN 83 is fainter than $G_{RP} = 15.5$ mag. In the FOV of MN 109, it is the source Gaia DR2 4322588299401926656 that allows us to conclude that our target is fainter than $G_{RP} = 18.5$ mag. These limits have been added to the measured magnitudes in Table 2.

For the other two objects, MN 108 and MN 112, we determined their magnitudes in the Johnson–Cousins BVR_CI_C photometry. We wish to point out that our I_C magnitudes are the first measurements for both objects. The observed B and V magnitudes from MN 112 are in good agreement with those reported in APASS. We note, however, that our BVR_C magnitudes for both objects deviate by 0.5−1.0 mag from the NOMAD photometric values listed in Gvaramadze et al. (2010a). This could suggest that the objects are photometric variables. All values are included in Table 2.

4.3. Imaging

The star MN 83 is particularly interesting because its K-band spectrum indicates an ionized gas nebula in addition to the elliptic
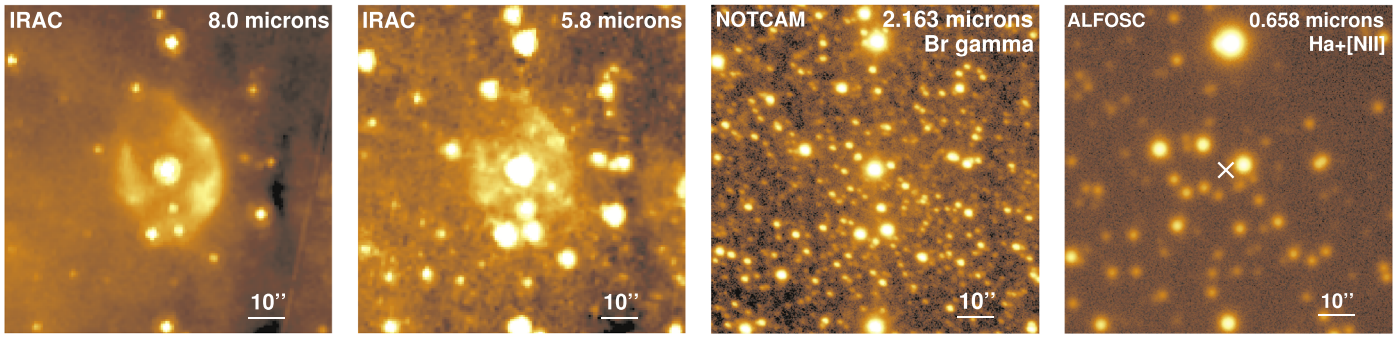
Figure 3. Images of the MN 83 nebula. From left to right: Spitzer IRAC 8.0 μm, Spitzer IRAC 5.8 μm, NOTCAM Brγ, and ALFOSC Hα+[N II]. On the IR images MN 83 is the brightest star in the middle. In the optical range (ALFOSC) the position of MN 83 is marked with the white cross. The intensity levels on individual frames are arbitrarily chosen to maximize the visibility of the nebula. The FOV of all frames is 1′.5 × 1′.5. North is up, east is left.
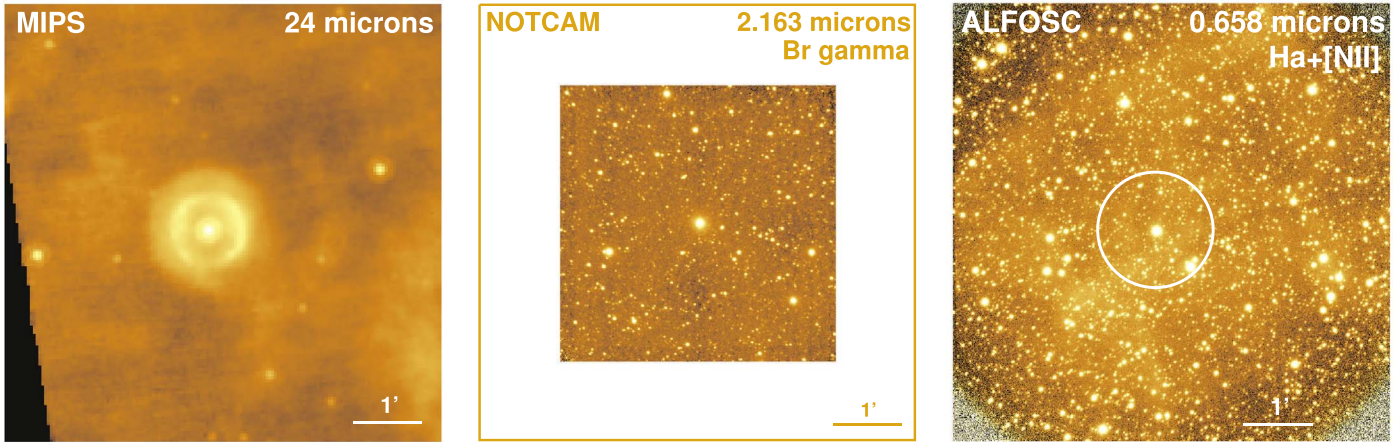

Figure 4. Images of the MN 112 nebula. From left to right: Spitzer MIPS 24 μm, NOTCAM Brγ, and ALFOSC Hα+[N II]. The MN 112 is the brightest star in the middle. The intensity levels on individual frames are arbitrarily chosen to maximize the visibility of the nebulae. The white circle in the ALFOSC image refers to the size and position of the circular nebula in 24 μm. North is up, east is left. The FOV of all frames is 6′.3 × 6′.3.

dusty nebula detected at 8 μm (Davies et al. 2007) and at 24 μm (Gvaramadze et al. 2010a). Therefore, we searched for further traces of the nebula at different wavelengths. First, we inspected all four bands of the IRAC frames at 3.6, 4.5, 5.8, and 8.0 μm. We found that the nebula is visible also at shorter wavelength than 8.0 μm, this being the frame where the nebula is brightest. In 5.8 and 4.5 μm the nebula gets progressively fainter until no detection at 3.6 μm. In Figure 3 we present the 8.0 and 5.8 μm frames. The nebula has a semimajor axis in the north–south direction with clearly brighter filaments toward the east and west. It is evident that in the north, approximately at the position angle of 25° (from north to east), the rim of the ellipse is broken or the material is significantly diluted so that the intensity of the emission dropped below the detection threshold compared to the rest of the nebula. The dimensions of the nebula at 8.0 μm are 44″ × 28″, slightly smaller than those at 24 μm. Without knowing the distance to MN83, no further calculations of, e.g., its physical size or age can be done.

Moving on to smaller wavelengths, we additionally opted to search for extended ionized gas structures in both Brγ 2.16 μm and Hα. The obtained images are included in Figure 3. No nebula has been detected at those wavelengths with the chosen total observing times of 30 minutes in Hα and 7.5 minutes in Brγ.

The second object of high interest is MN 112 owing to its previous classification as a cLBV and its intense emission-line spectra in both the optical and the near-infrared. Our optical image displays Hα + [N II] emission almost over the entire FOV

(right panel of Figure 4). However, in contrast to the sharp ring nebula seen at 24 μm on the MIPS image (left panel of Figure 4), the optical nebula appears to be smooth and with no clear substructure. Moreover, no pronounced emission was detected in the Brγ line (middle panel of Figure 4), nor was there any nebulosity or ring structure seen on the IRAC bands (not shown).

Neither MN 109 nor MN 109 shows any extended optical nebula.

5. Discussion

As mentioned in Section 1, central stars of dusty ring nebulae might correspond to a variety of massive stars in transition phases, and in terms of BSG central stars, B[e] supergiants and LBVs are the most likely candidates. In this section, we discuss the classification of our selected sample, based on their previous information and results obtained from their optical and K-band spectra.

5.1. CO Molecular Emission

None of the stars of our sample show CO bands. Of all B[e] SGs with observed K-band spectra, more than 65% display CO band emission (Kraus 2019). On the other hand, LBVs typically do not display CO band emission (e.g., Oksala et al. 2013), with one exception, the LBV star HR Car, which occasionally displays highly variable CO band emission (Morris et al. 1997). Therefore, the nondetection of warm CO
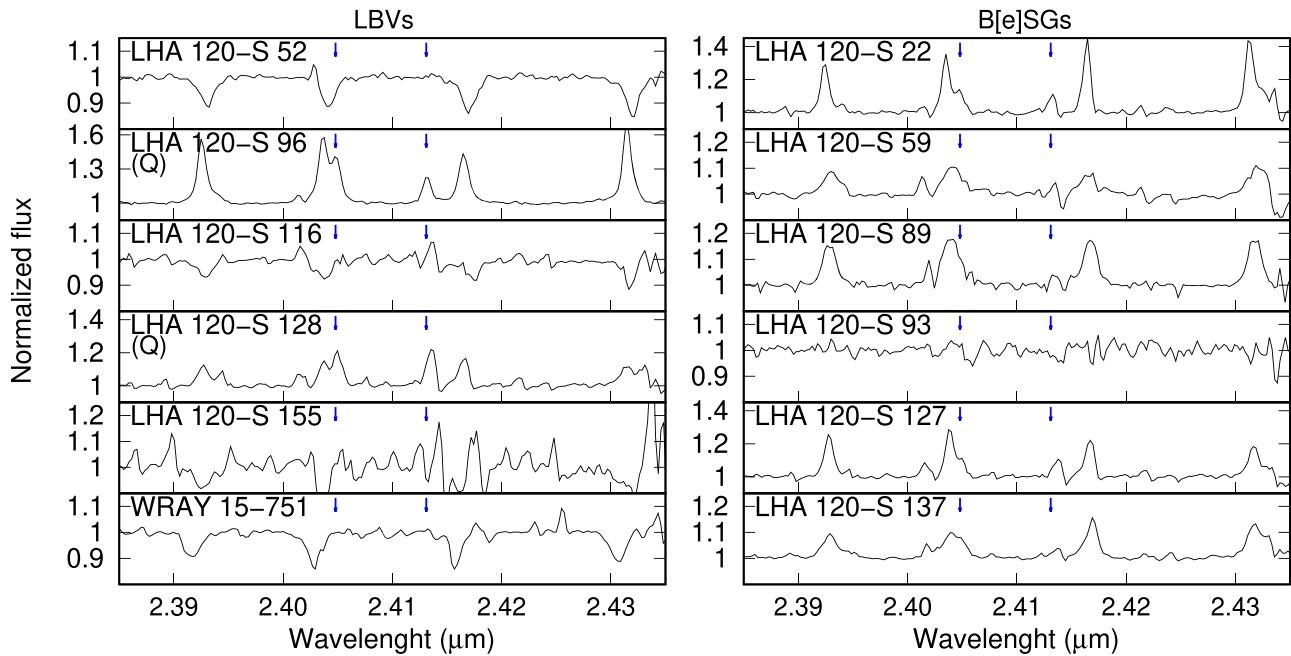
Figure 5. Yet-unpublished portion of the SINFONI spectra of the LBV and B[e]SG samples of Oksala et al. (2013), highlighting the positions of the Mg II 2.4047 and 2.4131 μm lines. The "Q" label identifies the LBVs in the quiescent state of their S Dor cycle.

emission in MN 83, MN 108, MN 109, and MN 112 is insufficient to distinguish between an LBV and a B[e]SG nature of the objects. Therefore, other characteristics should be considered.

5.2. On the IR Mg II Emission Lines

As mentioned in Section 2, MN 112 is considered a cLBV because its optical (low-resolution) spectrum resembles that of the confirmed LBV star P Cygni, and because of the similarity of its nebula with GAL 079.29+11.46 (Gvaramadze et al. 2010b). Hence, we could assume that MN 83 is also a cLBV because its IR spectrum displays many similarities to that of MN 112. Both objects present emission from the hydrogen Pfund series and from the Mg II 2.4047 and 2.4131 μm lines, and in both stars the Mg II lines are clearly more intense than the adjacent Pfund lines. In contrast, the star MN 109 shows weak and narrow Mg II lines in emission while the Pfund lines are in pure absorption, and MN 108 displays neither Pfund nor Mg II lines.

To check whether the lines of Mg II 2.4047 and 2.4131 μm are typically observed in emission in the spectra of LBV stars, we analyze the nonpublished spectral region around the Mg II doublet in the SINFONI spectra of the sample of LBVs and B[e]SGs from Oksala et al. (2013) (see Figure 5).

Of special interest for a comparison are hereby B[e]SGs with no CO band emission. Six B[e]SGs from the Magellanic Clouds were reported to display no CO band emission. Instead, all (except for LHA 120-S 93) show strong emission in the lines of the Pfund series (see Figure 2 of Oksala et al. 2013). From the LBV sample two objects, LHA 120-S 96 (=S Dor) and LHA 120-S 128, are in a quiescent state of their S Dor cycle and therefore display a very similar emission spectrum to the B[e]SGs. The other four LBVs appear to be in their outburst state, in which they display mostly absorption-line spectra resembling cool(er) supergiants. In these stars, the Pfund lines appear in absorption (see Figure 3 of Oksala et al. 2013).

We inspected the unpublished spectral ranges (longward of 2.4 μm) of these two samples of objects. They are displayed in Figure 5. The left panel contains the LBVs, and the right panel contains the B[e]SGs. The positions of the Mg II 2.4047 and 2.4131 μm lines are marked by the arrows. From this figure, we find that all B[e]SGs, except LHA 120-S 93, have the Mg II lines in emission, and in all of them, the intensity in the Mg II lines is considerably lower than in the adjacent Pfund lines. For the LBVs, we can see that the two objects in quiescence also have the Mg II lines in emission, and in one of them (LHA 120-S 128), the Mg II lines are more intense than the Pfund lines, similar to our two cLBV objects MN 83 and MN 112. Interestingly, at least three of the LBVs in outburst (LHA 120-S 116, LHA 120-S 155, WRAY 15–751) show an indication for emission in the Mg II lines, similar to our object MN 109. This suggests that MN 109 might be an LBV in a current outburst state. The rather low effective temperature, pointing toward an A-type supergiant star, seems to support such a classification.

LBVs have already been reported to display Mg II 2.4047 and 2.4131 μm lines in emission. In their infrared atlas of early-type stars, Lenorzer et al. (2002) present the spectra of three LBVs (η Carinae, AG Carinae, and P Cygni) showing these features (see their Figure 6). Moreover, the spectrum of P Cygni shows Mg II emission lines stronger than Pfund emission lines.

Clark et al. (2018) also presented K-band spectra for early-type stars of the Quintuplet cluster. They claimed that the Mg II lines in emission become prominent for spectral type B3 and later. Particularly, the three LBVs found in the cluster show Mg II 2.1369 and 2.1432 μm lines in emission. Only one of these spectra covers the region longward of 2.4 μm, and it also shows emission in Mg II 2.4047 and 2.4131 μm lines (see their Figures 1 and 7).

Of course, our rather qualitative analysis, based on just a small sample of stars, needs to be repeated in more depth and with a statistically significant sample of stars. Nevertheless, the intensity of the IR Mg II lines seems to be related to the density/extent of the circumstellar material and could be
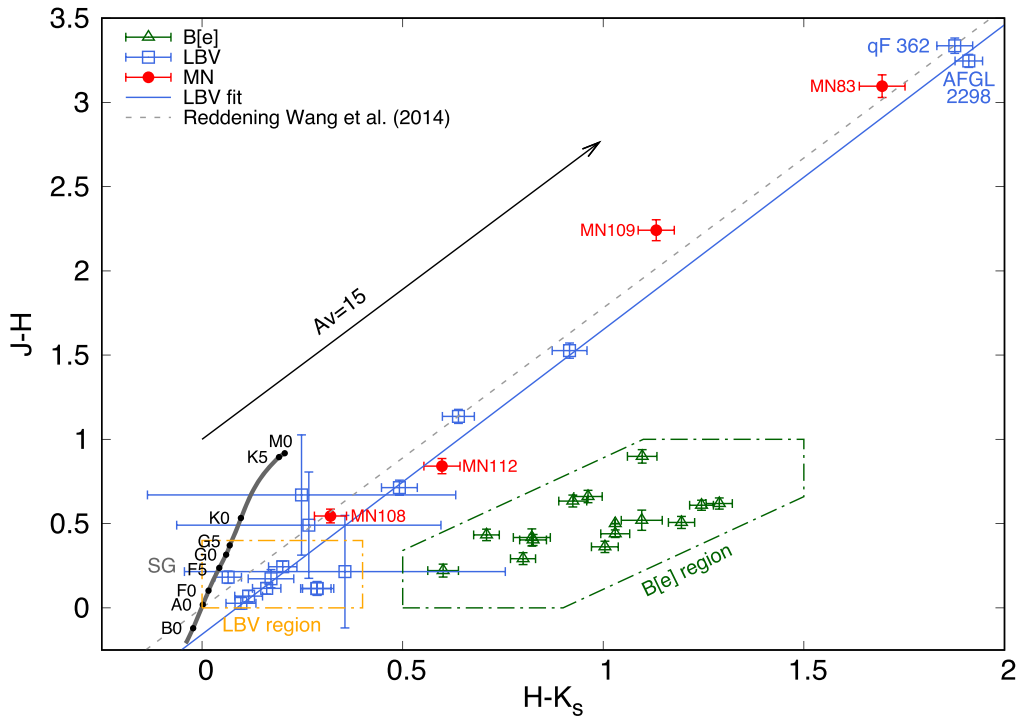
Figure 6. $J - H$ vs. $H - K_s$ color–color diagram. LBV and B[e]SG regions from Oksala et al. (2013) are plotted in orange and green, respectively. LBVs are plotted with blue squares, and the blue solid line is a linear fit to their positions. The reddening law obtained by Wang & Jiang (2014) is plotted as a dashed gray line, and a reddening vector for $A_v = 15$ is included. The position of the normal supergiant (SG) stars from spectral type O to M (Worthey & Lee 2011) are plotted in gray. The red circles mark the positions of our objects.

considered as a complementary criterion to classify stars as LBVs.

5.3. J − H versus H − K_s Color–Color Diagram

With the exception of the subtle distinction about the intensity of the IR emission lines of Mg II between LBV and B[e]SG stars highlighted in the previous section, the K-band spectra of quiescent LBVs are practically indistinguishable from those of B[e]SGs with no CO bands. However, these two groups of stars fall in different regions of a $J - H$ versus $H - K_s$ color–color diagram (Oksala et al. 2013), since the near-IR excess observed in B[e]SG arises from the warm/hot circumstellar dust, while the one in LBVs comes from free–free emission due to stellar winds. Thus, the IR color–color diagram can be used as additional diagnostics to discriminate between B[e]SGs and LBVs.

In Figure 6 we plot the IR color–color diagram and indicate the corresponding regions for LBVs (orange box) and B[e]SGs (green box) taken from Oksala et al. (2013). There, we plot with green triangles and blue squares the B[e] sample from Oksala et al. (2013) and the LBV stars listed in Clark et al. (2005), Aadland et al. (2019), and Campagnolo et al. (2018). The blue solid line is a linear fit of the position of confirmed LBVs in the $J - H$ versus $H - K_s$ diagram. This linear fit is in excellent agreement with the reddening law obtained by Wang & Jiang (2014, plotted with a dashed gray line). This law has been constructed from a sample of giant stars based on the NIR spectroscopic survey project APOGEE, by finding the relations between three NIR intrinsic colors and the effective temperature by fitting the bluest colors with a quadratic line. The red circles mark the positions of our four objects in this color–color diagram based on their 2MASS magnitudes (included in Table 2). All of them are distributed along the traced reddening

curve and in line with confirmed LBVs, implying that, depending on their intrinsic reddening values, their unreddened colors would place them in the box of confirmed LBVs or on the SG sequence.

Using the $E(B − V)$ values from the literature and assuming a total-to-selective extinction ratio $R_V = A_V/E(B − V) = 3.1$ (Schultz & Wiemer 1975), we obtained the corresponding extinction values A_V for the LBVs. For the two LBVs in the upper right corner of the diagram, we obtained $A_V = 24.8$ (for the upper, qF 362) and $A_V = 27.9$ (for the lower, AFGL 2298). With these values, we estimated the extinctions for our four objects. If we consider that MN 83 and MN 112 are cLBVs, their dereddened $J − H$ versus $H − K_s$ values should fall in the LBV region. With that restriction, we found lower limits of $A_V \sim 23$ for MN 83 and $A_V \sim 4$ for MN 112. In a similar way, if we deredden the position of MN 109 and MN 108 in the color–color diagram with the lower limit of A_V, i.e., when they cross the threshold of the LBV domain, we obtain $A_V \sim 16$ and $A_V \sim 5$, respectively. In the case of MN 109 the needed extinction is lower than that given by Phillips & Ramos-Larios (2008). The high extinction values obtained for MN 83 and MN 109 are consistent with the fact that both objects are not observed in the optical range.

6. Conclusions

We analyze four objects that have dusty envelopes resolved on Spitzer 24 μm images: [GKF 2010] MN 83, [GKF 2010] MN 108, [GKF 2010] MN 109, and [GKF 2010] MN 112. These objects have been suggested to host either a cLBV or a BSG central star.

To improve our knowledge on such massive stars in transition phases and on their surroundings, we obtained the first medium-resolution K-band spectra in the 2.3–2.47 μm

Cochetti et al.

region for these four objects, because this spectral region provides suitable information that can be used to classify evolved massive stars. For MN 108 and MN 112 we supplement the IR spectra with optical spectra and photometric BVR_CI_C measurements, as only these two stars have optical counterparts. We report the first I_C-band magnitudes of 13.521 ± 0.050 mag for MN 108 and 11.128 ± 0.024 mag for MN 112. We derived lower limits of $A_V > 16$ mag and $A_V > 23$ mag for MN 109 and MN 83, respectively, confirming their nondetections at optical wavelengths.

From our optical imaging, we found that none of the stars show Hα emission comparable to the infrared ring nebulae reported in the literature. However, MN 112 seems to be surrounded by extended, diffuse Hα emission, with approximately 2.5 times the size of the infrared ring nebula (Figure 4). Unfortunately, our Brγ images of MN 83 and MN 112 also do not show any extended emission, whereas clear emission from their dusty nebula is seen at 8 and 5.8 μm (Figure 3 for MN 83) and at 24 μm (Figure 4 for MN 112).

MN 83 and MN 112 show characteristics typically seen in LBV stars. The K-band spectra of both objects display intense IR Mg II lines in emission along with emission of the Pfund series, and they lack CO band emission. Their Mg II lines are more intense than the adjacent Pfund lines. Such a behavior is also seen in other LBV stars (see Section 5.2). The optical spectrum of MN 112 displays no [O I] emission, which would otherwise point to a B[e]SG classification. Moreover, the unreddened JHK colors place both stars in the loci of LBVs, so that a cLBV classification of both stars seems justified. One might speculate whether the dusty ring nebulae of these two objects might be remnants of either a giant eruption or S Dor cycle(s).

The situation for the other two objects is less clear. MN 109 seems to be an A-type supergiant star with $T_{\rm eff} \leqslant 10{,}000$ K and $\log g \simeq 3$. Its K-band spectrum displays the Pfund lines in absorption along with weak emission of the IR Mg II lines, similar to LBVs in outburst. Hence, MN 109 could be considered as a cLBV star in its active phase.

The optical spectrum of MN 108 reveals narrow photospheric lines of H I, He I, and He II characteristic for a hot, O-type supergiant. The K-band spectrum displays only Si IV emission, in agreement with the classification of an O-type supergiant, but is otherwise featureless. The absence of pronounced wind lines in the optical spectrum might suggest that the star is a regular, non-LBV object. Whether the dusty envelope (the witness of a phase of intense mass loss) might still be a remnant from a prior red supergiant phase can be neither confirmed nor excluded, but requires further investigation.

Facilities: Gemini:Gillett(GNIRS), NOT, VLT:Yepun.
Software: IRAF (Tody 1986).

ORCID iDs

Yanina R. Cochetti ⓘ https://orcid.org/0000-0002-2763-7250
Michaela Kraus ⓘ https://orcid.org/0000-0002-4502-6330
Tiina Liimets ⓘ https://orcid.org/0000-0003-2196-9091
Anlaug A. Djupvik ⓘ https://orcid.org/0000-0001-6316-9880

References

Aadland, E., Massey, P., Neugent, K., & Drout, M. 2019, AAS Meeting, 233, 353.05
Allen, D. A., & Glass, I. S. 1976, ApJ, 210, 666
Aret, A., Kraus, M., Muratore, M. F., & Borges Fernandes, M. 2012, MNRAS, 423, 284
Aret, A., Kraus, M., & Šlechta, M. 2016, MNRAS, 456, 1424
Arias, M. L., Cidale, L. S., Kraus, M., et al. 2018, PASP, 130, 114201
Becker, R. H., White, R. L., Helfand, D. J., & Zoonematkermani, S. 1994, ApJS, 91, 347
Campagnolo, J. C. N., Borges Fernandes, M., Drake, N. A., et al. 2018, A&A, 613, A33
Cannon, A. J. 1924, BHarO, 801, 1
Cidale, L. S., Borges Fernandes, M., Andruchow, I., et al. 2012, A&A, 548, A72
Clark, J. S., Castro, N., Garcia, M., et al. 2012, A&A, 541, A146
Clark, J. S., Egan, M. P., Crowther, P. A., et al. 2003, A&A, 412, 185
Clark, J. S., Larionov, V. M., & Arkharov, A. 2005, A&A, 435, 239
Clark, J. S., Lohr, M. E., Patrick, L. R., et al. 2018, A&A, 618, A2
Condon, J. J., Cotton, W. D., Greisen, E. W., et al. 1998, AJ, 115, 1693
Conti, P. S. 1997, in ASP Conf. Ser. 120, Luminous Blue Variables: Massive Stars in Transition, ed. A. Nota & H. Lamers (San Francisco, CA: ASP), 387
Davies, B., Figer, D. F., Kudritzki, R.-P., et al. 2007, ApJ, 671, 781
de Wit, W. J., Oudmaijer, R. D., & Vink, J. S. 2014, AdAst, 2014, 270848
Fazio, G. G., Hora, J. L., Allen, L. E., et al. 2004, ApJS, 154, 10
Feast, M. W., Thackeray, A. D., & Wesselink, A. J. 1960, MNRAS, 121, 337
Georgy, C. 2012, A&A, 538, L8
Glass, I. S. 1977, MNRAS, 178, 9P
Groh, J. H., Damineli, A., & Hillier, D. J. 2008, RMxAC, 33, 132
Gvaramadze, V. V., Kniazev, A. Y., & Fabrika, S. 2010a, MNRAS, 405, 1047
Gvaramadze, V. V., Kniazev, A. Y., Fabrika, S., et al. 2010b, MNRAS, 405, 520
Gvaramadze, V. V., Kniazev, A. Y., Miroshnichenko, A. S., et al. 2012, MNRAS, 421, 3325
Gvaramadze, V. V., & Menten, K. M. 2012, A&A, 541, A7
Henize, K. G. 1956, ApJS, 2, 315

Hubeny, I., & Lanz, T. 2011, Synspec: General Spectrum Synthesis Program, Version 51, Astrophysics Source Code Library, ascl:1109.022

Jester, S., Schneider, D. P., Richards, G. T., et al. 2005, AJ, 130, 873

Kastner, J. H., Buchanan, C., Sahai, R., Forrest, W. J., & Sargent, B. A. 2010, AJ, 139, 1993

Kastner, J. H., Buchanan, C. L., Sargent, B., & Forrest, W. J. 2006, ApJL, 638, L29

Kohoutek, L., & Wehmeyer, R. 1999, A&AS, 134, 255

Kourniotis, M., Kraus, M., Arias, M. L., Cidale, L., & Torres, A. F. 2018, MNRAS, 480, 3706

Kraus, M. 2017, in ASP Conf. Ser. 508, The B[e] Phenomenon: Forty Years of Studies, ed. A. Miroshnichenko et al. (San Francisco, CA: ASP), 219

Kraus, M. 2019, Galax, 7, 83

Kraus, M., Arias, M. L., Cidale, L. S., & Torres, A. F. 2020, MNRAS, 493, 4308

Kraus, M., Borges Fernandes, M., & de Araújo, F. X. 2007, A&A, 463, 627

Kraus, M., Borges Fernandes, M., & de Araújo, F. X. 2010, A&A, 517, A30

Kraus, M., Cidale, L. S., Arias, M. L., Oksala, M. E., & Borges Fernandes, M. 2014, ApJL, 780, L10

Kraus, M., Krügel, E., Thum, C., & Geballe, T. R. 2000, A&A, 362, 158

Kraus, M., Liimets, T., Cappa, C. E., et al. 2017, AJ, 154, 186

Kraus, M., Oksala, M. E., Nickeler, D. H., et al. 2013, A&A, 549, A28

Kurucz, R. L. 1979, ApJS, 40, 1

Langer, N. 2012, ARA&A, 50, 107

Langer, N., Hamann, W.-R., Lennon, M., et al. 1994, A&A, 290, 819

Leitherer, C., & Robert, C. 1991, ApJ, 377, 629

Lenorzer, A., Vandenbussche, B., Morris, P., et al. 2002, A&A, 384, 473

Liermann, A., Schnurr, O., Kraus, M., et al. 2014, MNRAS, 443, 947

Maeder, A., Lequeux, J., & Azzopardi, M. 1980, A&A, 90, L17

Maravelias, G., Kraus, M., Cidale, L. S., et al. 2018, MNRAS, 480, 320

Marston, A. P., & McCollum, B. 2008, A&A, 477, 193

McGregor, P. J., Hillier, D. J., & Hyland, A. R. 1988, ApJ, 334, 639

Meilland, A., Kanaan, S., Borges Fernandes, M., et al. 2010, A&A, 512, A73

Menzel, D. H., Aller, L. H., & Baker, J. G. 1938, ApJ, 88, 313

Meynet, G., Georgy, C., Hirschi, R., et al. 2011, BSRSL, 80, 266

Meynet, G., & Maeder, A. 2005, A&A, 429, 581

Morris, P. W., Eenens, P. R. J., Hanson, M. M., Conti, P. S., & Blum, R. D. 1996, ApJ, 470, 597

Morris, P. W., Voors, R. H. M., Lamers, H. J. G. L. M., & Eenens, P. R. J. 1997, in ASP Conf. Ser. 120, Luminous Blue Variables: Massive Stars in Transition, ed. A. Nota & H. Lamers (San Francisco, CA: ASP), 20

Nazé, Y., Rauw, G., & Hutsemékers, D. 2012, A&A, 538, A47

Nota, A., Livio, M., Clampin, M., & Schulte-Ladbeck, R. 1995, ApJ, 448, 788

Oksala, M. E., Kraus, M., Cidale, L. S., Muratore, M. F., & Borges Fernandes, M. 2013, A&A, 558, A17

Phillips, J. P., & Ramos-Larios, G. 2008, MNRAS, 387, 407

Puls, J., Vink, J. S., & Najarro, F. 2008, A&ARv, 16, 209

Rieke, G. H., Young, E. T., Engelbracht, C. W., et al. 2004, ApJS, 154, 25

Robberto, M., & Herbst, T. M. 1998, ApJ, 498, 400

Schultz, G. V., & Wiemer, W. 1975, A&A, 43, 133

Smith, H. J. 1957, PASP, 69, 137

Smith, N. 2007, AJ, 133, 1034

Smith, N. 2014, ARA&A, 52, 487

Stahl, O., Jankovics, I., Kovács, J., et al. 2001, A&A, 375, 54

Stahl, O., Leitherer, C., Wolf, B., & Zickgraf, F. J. 1984, A&A, 131, L5

Stahl, O., Wolf, B., Zickgraf, F. J., et al. 1983, A&A, 120, 287

Stringfellow, G. S., Gvaramadze, V. V., Beletsky, Y., & Kniazev, A. Y. 2012, in ASP Conf. Ser. 465, Proc. of a Scientific Meeting in Honor of Anthony F. J. Moffat, ed. L. Drissen et al. (San Francisco, CA: ASP), 514

Tody, D. 1986, Proc. SPIE, 627, 733

van Genderen, A. M., de Groot, M., & Sterken, C. 1997, A&AS, 124, 517

Wachter, S., Mauerhan, J. C., Van Dyk, S. D., et al. 2010, AJ, 139, 2330

Wang, S., & Jiang, B. W. 2014, ApJL, 788, L12

Weis, K. 2001, RvMA, 14, 261

Wheelwright, H. E., de Wit, W. J., Weigelt, G., Oudmaijer, R. D., & Ilee, J. D. 2012, A&A, 543, A77

Worthey, G., & Lee, H.-c 2011, ApJS, 193, 1

Zickgraf, F. J., Wolf, B., Stahl, O., Leitherer, C., & Klare, G. 1985, A&A, 143, 421